Global Sensitivity Analysis of the L-MEB Model for Retrieving Soil Moisture

Zengyan Wang, Tao Che, *Member, IEEE*, and Yuei-An Liou, *Senior Member, IEEE*

***Abstract*—A global sensitivity analysis utilizing the extended Fourier amplitude sensitivity test is used to determine the parameter sensitivity of the L-band microwave emission of the biosphere (L-MEB) model. The results are analyzed from two perspectives of calibration and inversion. First, the parameters of surface soil moisture, soil roughness factor, vegetation optical depth at nadir, and effective land surface temperature are the four most sensitive parameters in the L-MEB model, demonstrating their possibility to be retrieved in the multiparameter retrieval approaches. Then, the high total sensitivity index (TSI) values of surface soil temperature in the analyses emphasize the importance of high-precision land surface temperature data in the surface soil moisture retrievals, especially for rougher or more vegetated surface conditions. Finally, our analysis indicates that TSI values are high for the soil surface roughness and vegetation optical depth model parameters but low for the vegetation structure, single scattering albedo, and soil roughness coefficient model parameters at incidence angles near nadir. This suggests that calibration experiments performed at small incidence angles may be appropriate for some but not all of the model parameters, which characterize the effect of soil surface roughness and vegetation on the terrestrial brightness temperature. Consequently, new calibration procedures that account for the different relative sensitivities of these model parameters at larger incidence angles may need to be developed in the future.**

***Index Terms*—Global sensitivity analysis (SA), L-band microwave emission of the biosphere (L-MEB), passive microwave remote sensing, soil moisture.**

Manuscript received November 17, 2014; revised May 7, 2015, September 30, 2015, and November 26, 2015; accepted December 9, 2015. Date of publication January 21, 2016; date of current version March 25, 2016. This work was supported by the Chinese National Natural Science Foundation under Grants 91125001 and 41271356, the Chinese Academy of Sciences Project KZCX2-XB3-15, and the Ministry of Science and Technology under Grants MOST 103-2111-M-008-023 and 103-2221-E-008-074.

Z. Wang is with the Key Laboratory of Remote Sensing of Gansu Province, Cold and Arid Regions Environmental and Engineering Research Institute, Chinese Academy of Sciences, Lanzhou 730000, China, and also with the University of Chinese Academy of Sciences, Beijing 100049, China.

T. Che is with the Heihe Remote Sensing Experimental Research Station, Cold and Arid Regions Environmental and Engineering Research Institute, Chinese Academy of Sciences, Lanzhou 730000, China, and also with the Center for Excellence in Tibetan Plateau Earth Sciences, Chinese Academy of Sciences, Beijing 100101, China (e-mail: chetao@lzb.ac.cn).

Y.-A. Liou is with the Center for Space and Remote Sensing Research, National Central University, Taoyuan 32001, Taiwan, the Taiwan Geographic Information System Center, Taipei 10092, Taiwan, and also with the Taiwan Group on Earth Observations, Hsinchu 30274, Taiwan (e-mail: yueian@csrsr.ncu.edu.tw).

Digital Object Identifier 10.1109/TGRS.2015.2509176

I. Introduction

SURFACE soil moisture is an important variable in many hydrological, meteorological, and climate models [1]–[5]. L-band micrometer radiometry has been shown to be one of the most promising remote sensing techniques used to monitor surface soil moisture at large scales [6]–[12]. The European Space Agency's Soil Moisture and Ocean Salinity (SMOS) mission, launched in November 2009, is the first satellite aiming at surface soil moisture monitoring using the L-band, and its baseline payload is an L-band (1.4 GHz) 2-D interferometric radiometer [13]. Until now, various soil moisture retrieval results based on SMOS observation have been obtained, and their accuracy has been accessed through both field observations and other satellite-based soil moisture products [14], [15]. However, the accuracy is reported to be varying depending on area and RFI levels [16]. The newest satellite mission of the Soil Moisture Active Passive (SMAP) has already been launched on January 31, 2015. Its architecture includes an L-band radar (1.26 GHz) and an L-band (1.41 GHz) radiometer and aims to provide new soil moisture estimations at a finer grid resolution of $\sim$10 km [17].

A number of land surface and radiative transfer models for the passive microwave remote sensing of surface soil moisture have been developed, and they can be categorized as either biophysical or empirical/semiempirical models. The biophysical ones [1], [2], [18]–[24] characterize many physical parameters dominating microwave emission from the land surface and thus are able to examine the sensitivity of various frequencies and techniques for soil moisture retrievals through remote sensing in bare or vegetated areas [11], [12], [25]–[28]. The empirical/semiempirical ones simplify the radiative transfer process by fitting between physical model simulations and actual observations and thus are of practical use for large-scale and operational applications [29]–[31]. Currently, for the simplification and accuracy in the surface soil moisture estimations, a dedicated semiempirical radiative transfer model of the L-band microwave emission of the biosphere (L-MEB) was developed as the core of the processor in dealing with the SMOS and SMAP passive microwave observations [31].

There are many empirical or semiempirical parameters, such as Q_R, H_R, τ, and ω in the L-MEB model (Table I) [32], [33], which are distinct to different land surface types and thus should be calibrated first before the retrieval process. Before and after the launch of SMOS, several ground-based or airborne experiments were carried out to conduct the calibration or evaluation of the L-MEB model in different regions and on different spatial scales [31], [34]–[40]. However, due to the nature of

0196-2892 © 2016 IEEE. Personal use is permitted, but republication/redistribution requires IEEE permission.
See http://www.ieee.org/publications_standards/publications/rights/index.html for more information.

TABLE I
LIST OF L-MEB MODEL PARAMETERS INCLUDED IN THE GLOBAL SA

Input Parameter	Definition	Type	Default value	Value range
SM	Surface soil moisture, m^3/m^3	variable	0.3	0-0.5
H_R	Soil roughness factor	variable	0.6	0-1.1
N_R	Soil roughness coefficient	empirical	0	-2-2
τ_{NAD}	Vegetation optical depth	variable	0.3	0-0.5
tt	Vegetation structure factor	empirical	1	1-10
ω	single scattering albedo	empirical	0.05	0-0.1
T_{eff}	Effective land surface temperature, ℃	variable	25	0-40
$Vclay$	Clay content, %	variable	30	0-70

the semiempirical model, the calibrated results in particular locations and on particular scales need more verification before they can be applied to other places and on different spatial resolutions [31], [41]. As a result, a thorough and quantitative understanding of the L-MEB model and its parameters, namely, the model's parameter sensitivity analysis (SA), is of great importance to understand the existing calibrated results and to instruct the future work when more calibration experiments are conducted in other places.

Multiangle and multipolarization passive microwave observations in the SMOS and SMAP configurations have made it possible to retrieve multiple parameters in the L-MEB model simultaneously. The "3-P" approach [31], in which the three parameters of surface soil moisture (*SM*, m^3/m^3), vegetation optical depth (τ), and soil roughness factor (H_R) are retrieved simultaneously, is proposed as the default method to retrieve *SM* in the SMOS data processor [31]. Until now, much of the validation research has been conducted based on field experiments, and the *SM* retrieval accuracy on different resolutions of tens to thousands of meters is found to be from 0.02 to 0.1 m^3/m^3 [16], [41], [42]. However, in this "3-P" method, the accuracy of the retrieved *SM* values depends largely on the initial values and their searching ranges of τ and H_R, as well as the accuracy of other input parameters. As a result, to discuss the systematic error sources and the possible improvements to the traditional "3-P" approach, a numerical SA of the L-MEB model is still needed. An additional benefit is an overall understanding of the multiparameter retrieval method.

There are two types of SA methods: local and global [43]. The local methods are used to calculate the sensitivity of one parameter while holding other parameters fixed to a normal value. The global methods are characterized by obtaining the sensitivity measures of many parameters at one time by exploring the multidimensional parameter space. Until now, many SA works have been published based on the traditional local SA method [44]–[46], which is appropriate to examine the sensitivity of individual parameters. Currently, more attention has been paid to the global ones [47], [48]. Ma *et al.* [47] have applied the global method to analyze the parameters in the advanced integral equation model and to get a better understanding of scatting for active microwave soil moisture retrievals. Neelam and Mohanty [48] applied a similar global method to analyze the parameters in one zero-order radiative transfer model, and they focused on the interaction between parameters. In this paper, a global sensitivity approach of the extended Fourier amplitude sensitivity test (eFAST) [49] is adopted. The interactions and comparisons of the different parameter sensitivities in the L-MEB model are then analyzed accordingly to instruct the application of the model in future calibration activities and ultimately retrievals from satellites.

This paper covers an introduction to the L-MEB model and eFAST method. Then, the parameters of interest are summarized, and the design of three SA tests is described. The SA results are then discussed from the perspectives of calibration and inversion. Finally, the results of the research are summarized and concluded.

II. MODEL AND METHOD

A. L-MEB Model

The L-MEB model is a simplified radiative transfer model. It represents the land surface with two homogenous layers, namely, soil and vegetation. It uses the semiempirical Q-H model to predict the reflection at the vegetation–soil interface and adopts the $\tau-\omega$ model to simulate the radiation transfer between soil and vegetation. The Q-H model is expressed as [31]

$$r_{GP}(\theta)=\left[(1-Q_R)r^*_{GP}(\theta)+Q_R r^*_{GQ}(\theta)\right]\exp\left(-H_R\cos^{N_{RP}}(\theta)\right) \quad (1)$$

where r_G and r^*_G are the reflectivity of the rough and smooth soil surfaces, respectively, and the subscripts P and Q represent horizontal and vertical polarizations, respectively. H_R and N_R are two best-fit parameters used to simulate the effect of roughness conditions. Q_R is a polarization mixing parameter, and its value is very small at the L-band [36]–[38], [50]. r^*_G is calculated as a function of the incidence angle (θ) and soil permittivity (ε) according to the Fresnel equation. ε can be

computed as a function of surface soil moisture (*SM*, m^3/m^3) and several soil texture parameters including bulk soil density (ρ_b, g/cm^3), sand content ($V_{\rm sand}$, %), clay content ($V_{\rm clay}$, %), and soil temperature (T_S, °C) based on the established dielectric model, such as Dobson [51], Liou and England [18], or Mironov *et al.* [52]. In this paper, the Mironov model is chosen for the fewest input parameters of clay percentage ($V_{\rm clay}$, %) and *SM*.

The $\tau-\omega$ model is expressed as [31]

$$T_{BP} = (1-\omega_P)(1-\gamma_P)T_V + (1-\omega_P)(1-\gamma_P)T_V r_{GP}\gamma_P + (1-r_{GP})\gamma_P T_S \quad (2)$$

where r_G is the soil reflectivity, the subscript P represents the polarization of H or V, T_S(K) and T_V(K) are the effective soil and vegetation temperature, respectively, and ω is the single scattering albedo used to parameterize the vegetation scattering properties. The transmission factor γ is calculated from a more popular parameter called vegetation optical depth (τ) by

$$\gamma_P = \exp(-\tau_P/\cos\theta) \quad (3)$$

where the subscript P still represents the polarization of H or V.

Among all of the aforementioned parameters of the L-MEB model, T_S, T_V, and τ require further elaboration. For T_S, the vertical profiles of soil moisture and temperature should be taken into consideration due to the penetration capability of the L-band radiation. A simplified semiempirical equation is used in L-MEB [36], [53]. Most previous studies assume that the value of T_V, effective vegetation temperature, was approximately equal to that of T_S [54]. This assumption is acceptable while applying to SMOS data, with an overpass at the local time of around 6:00 A.M. and 6:00 P.M. when close to a minimal gradient in temperature is found. However, it should be noted that, during the daytime, the temperature gradients are always large and the assumption then becomes invalid. Some modifications should be made in this situation, which is common for many airborne experiments. In L-MEB, another parameter of effective land surface temperature $T_{\rm eff}$ is proposed as

$$T_{\rm eff} = A_t T_V + (1-A_t)T_S \quad (4)$$

with

$$A_t = B_t\left(1-\exp(-\tau_{\rm NAD})\right) \text{ and } A_t \le 1 \quad (5)$$

where the parameters A_t and B_t account for the effect of the vegetation structure with $B_t = 1.7$ as its default value. In this paper, an assumption $T_{\rm eff} \approx T_V \approx T_S$ is used for simplification.

Regarding the optical depth τ of standing vegetation, many researches have verified the linear relationship between $\tau_{\rm NAD}$ ($\tau_{\rm NAD}$ is the value of τ at nadir) and the total vegetation water content ($V_{\rm WC}$, kg/m^2) [55], modeled as follows: $\tau_{\rm NAD} = b \times V_{WC}$ [56]. The value of the b parameter is related to vegetation types [57]. As it is difficult to estimate $V_{\rm WC}$ by means of remote sensing on a large scale, another parameterization of τ as a function of the leaf area index (LAI) is proposed as follows: $\tau_{\rm NAD} = b' \times LAI + b''$ (b' and b'' are two empirical parameters) and is used in the SMOS soil moisture retrievals [31]. In L-MEB, the effect of vegetation structure on $\tau_{\rm NAD}$ is considered according to

$$\tau_H(\theta) = \tau_{\rm NAD}\left(\sin^2(\theta)\times tt_H + \cos^2(\theta)\right)$$
$$\tau_V(\theta) = \tau_{\rm NAD}\left(\sin^2(\theta)\times tt_V + \cos^2(\theta)\right) \quad (6)$$

where tt_H and tt_V are two parameters accounting for the dependence of τ on vegetation structure. For isotropic vegetation, $tt_H = tt_V = 1$.

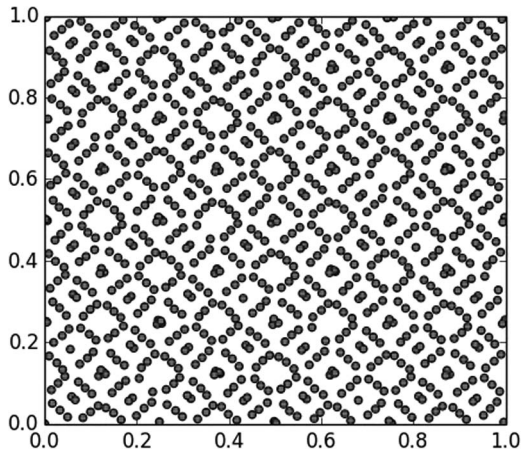

Fig. 1. Numerical example of the eFAST sampling (1000 sample points in a two-input-parameter case) based on the Fourier transformation functions in (7).

B. eFAST Method

The eFAST method, an extension of the classic FAST method [49], is a global, quantitative, and variance-based method of SA. It combines the better sampling efficiency of the FAST method as compared to the Monte Carlo approaches [58] with the Sobol' ability in considering the interactions among different parameters [59] and is of great use in understanding the complex nonlinear and nonmonotonic models. In recent years, the eFAST method has been applied in many hydrological and ecological models [60], [61].

For any model simplified as $y = f(x)$, $x = (x_1, x_2, \ldots, x_n)$ to be analyzed in the eFAST method, with the parameters x_1 to x_n representing the total set of the n input parameters, the multidimensional parameter space should be first converted into a 1-D space through the Fourier transformation functions named the searching curves as

$$x_i(s) = \frac{1}{2} + \frac{1}{\pi}\arcsin\left(\sin(\omega_i s + \varphi_i)\right) \quad (7)$$

where $i = 1, 2, \ldots, n$, φ_i is a random phase shift in $[0, 2\pi)$, and s represents the sample order varying from 1 to the total number of samples (N_s). ω_i is the Fourier frequency to be properly selected for each parameter. The selection of a set of values within the value ranges for each parameter in this procedure is called resampling, as shown in Fig. 1 with $N_s = 1000$ in a

two-input-parameter case based on the transformation in (7). The key to this procedure is the selection of some critical parameters such as ω_i and N_s, which are elaborated in detail in Saltelli [49]. Briefly speaking, the minimum total sample size N_s is defined as follows: $N_s = (2M\omega_{\max} + 1)N_r$, where M is the given interference factor, $\omega_{\max}$ is the largest value among the set of ω_i, and N_r is the number of searching curves (with different φ values). Once the sample size N_s is given, the recommended values of ω_i and N_r can be chosen according to a simple rule as the ratio ω_i/N_r varies between 16 and 64.

Then, in the second procedure, the main sensitivity index (MSI) and total sensitivity index (TSI) of each input parameter are calculated through the Fourier amplitude sensitivity test. In this procedure, the sample values in the first procedure are taken into the model, and the model results are transformed in its Fourier series expansion of

$$y = f(s) = \sum_{j=-\infty}^{+\infty} \{A_j \cos js + B_j \sin js\} \tag{8}$$

where $j \in Z = \{-\infty, \ldots, -1, 0, 1, \ldots, +\infty\}$ and A_j and B_j are two Fourier coefficients expressed as

$$A_j = \frac{1}{2\pi} \int_{-\pi}^{\pi} f(s) \cos(js) ds$$

$$B_j = \frac{1}{2\pi} \int_{-\pi}^{\pi} f(s) \sin(js) ds. \tag{9}$$

Then, the total variance D of the model output is obtained by

$$D = \frac{1}{2\pi} \int_{-\pi}^{\pi} f^2(s) ds - \left[\frac{1}{2\pi} \int_{-\pi}^{\pi} f(s) ds \right]^2 \approx 2 \sum_{j=1}^{+\infty} \left(A_j^2 + B_j^2 \right). \tag{10}$$

The partial variance D_i of the individual parameter x_i is calculated based on the Fourier coefficients A_j and B_j with respect to its specific Fourier frequency ω_i as

$$D_i = \sum_{j=-\infty}^{+\infty} \Lambda_{j\omega_i} = 2 \sum_{j=1}^{+\infty} \left(A_{j\omega_i}^2 + B_{j\omega_i}^2 \right) \tag{11}$$

where Λ is the spectrum of the Fourier series expansion defined as $\Lambda_j = A_j^2 + B_j^2$.

Finally, the main and total sensitivity results of MSI and TSI for the parameter x_i are expressed in the following, respectively

$$\text{MSI} = \frac{D_i}{D}$$

$$\text{TSI} = 1 - \frac{D_{-i}}{D} \tag{12}$$

where D_{-i} is the partial variance of all other parameters, but x_i, expressed as $D_{-i} = \sum D_k, k \neq i$.

The calculations of TSI and MSI are based on the principle that the fraction of the variance D explained by a specific parameter is proportional to the Fourier coefficient with its corresponding frequency and its multiples. Compared to the traditional FAST sensitivity parameter of MSI, the new eFAST sensitivity parameter of TSI takes the interaction effects between the other parameters and the analyzed parameter into consideration other than the effect of the analyzed parameter only on the final sensitivity results, making it a more effective index to be discussed in the SA. It should be noted that the MSI values of all input parameters sum to close to 1, while the total TSI value of all of the parameters could be higher than 1 for the interaction effect consideration. The differences will be further elaborated in the following results and discussion in Section IV.

III. Parameter SA Tests

A. Parameters

To conduct the eFAST SA tests, a general and quantitative understanding of the parameters in the L-MEB model is needed. Table I summarizes the main parameters and their variation ranges in the L-MEB model.

For the soil-related parameters, such as Q_R, H_R, and N_R, the value of Q_R was set to be 0 at the L-band in accordance with the previous studies [36]–[38], [50]. The SMOS default value of H_R was set to be about 0.2 for smooth surfaces and around 0.6 for rough surfaces [31]. However, the parameterization results of H_R with NAFE'05 data suggest that the values of H_R proposed for SMOS might be too low, and the new calibrated H_R values are between about 0.38 and 0.87 [41]. Wigneron *et al.* [38] developed a new calibration method relating the roughness parameters, including H_R, with the standard deviation of the surface height (S_D), and it was found that the calibrated values of H_R increased from about 0.1 for $S_D = 5$ mm to about 1.1 for $S_D = 50$ mm. Furthermore, the dependence of H_R on the value of *SM* was also found in several previous studies [34], [36], [37], [41], while Escorihuela *et al.* [62] suggested that this relationship may be due to the difference between the sampling depth (0–5 cm) of the ground-based soil moisture measurements and the typical responding depth (0–2 cm) of an L-band microwave radiometer under wet conditions. Thus, the dependence of H_R on *SM* is still uncertain. The values of N_R were set to vary between -2 and 2, and they differed in polarizations [16], [37]. Results also indicated that the effect of N_R on *TB* was stronger at larger incidence angles [38]. More recent studies focused on the parameterization of the difference $(N_{\text{RH}} - N_{\text{RV}})$ by surface roughness parameters, such as the standard deviation of the height (S_D) or the correlation length (Z_S). The difference was found to be about 2 for smooth surfaces and near 0 for rough surfaces [38]–[40].

For the vegetation-related parameters, the calibration results of tt_H and tt_V were closely related to the vegetation types [31]. The value of ω was found to be around 0.05 for both corn and grass, and the abnormal value of 0.15 in the BARC experiment might be due to the larger incidence angles (up to 70°) or errors in the calibration results of H_R [34]. As a result, a variation range of 0–0.1 for ω is provided in Table I. Additionally, the variation range of τ_{NAD} is given as 0–0.5 in Table I, corresponding to the low vegetation covers including most agriculture crops and grasses. In this paper, all of the

discussions about vegetation covers are confined to the scope of these low vegetation covers other than tall woods and forest.

B. SA Tests

Using the parameters and their variation ranges of the L-MEB model given in Table I, three SA tests are designed according to the different sets of input parameters to be analyzed in the eFAST method.

Test 1—Parameters' Sensitivity Comparison Analysis: In the test, all parameters in Table I are included in the eFAST method, and their sensitivities (TSI and MSI values), in terms of each parameter's relative importance on the terrestrial brightness temperature as predicted by the L-MEB model, are analyzed to discover the primary sensitive factors in the L-MEB model at different incidence angles and polarizations. The differences between the two sensitivity indexes are also compared to discuss the parameter interaction effects on the total sensitivity results.

Test 2—Parameters' Sensitivity Variation Analysis: In this test, all parameters but H_R or τ_{NAD} in Table I are included in the eFAST method, and their sensitivities are calculated under different roughness or vegetation conditions. The TSI variations of these parameters are then analyzed to discuss the possible error resources and the potential improvements to the current multiparameter retrieval method.

Test 3—Calibration Parameters' SA: In this test, all of the parameters that need to be calibrated in the L-MEB model are included in the eFAST method, and the other parameters are set constant with the default values given in Table I. The sensitivities of the calibration parameters and their changes are analyzed under different soil moisture conditions to investigate the reliability of the current calibration method of iteration based on the observed brightness temperature (*TB*, K) and *SM* values.

IV. Results and Discussion

A. Test 1: Parameters' Sensitivity Comparison Analysis

In this test, all parameters in Table I are analyzed in the eFAST method. Both the TSI and MSI values represent the sensitivity of the model results to the parameter variations, and the higher TSI/MSI values indicate the higher ability of that parameter to be retrieved in the inversion. Figs. 2 and 6 show the TSI, MSI, and their differences of all of these parameters at four different incidence angles of 5°, 20°, 40°, and 60° for two different land cover types of bare soils (Fig. 2) and vegetation covers (Fig. 6). Tables II and III then list the numerical values of the two indexes in these experiments. In the following discussions, all of the analyses are made on each land cover type separately.

1) Test 1 for Bare Soils: The differences of the two sensitivity indexes of TSI and MSI in the eFAST method can be clearly observed in Fig. 2 and Table II that 1) for the nonlinear L-MEB model, the total values of MSI of all parameters sum to about 0.9, while the total values of TSI are a bit higher than 1; 2) comparing with MSI, the interaction effects among parameters just increase the sensitivity results of TSI, and both TSI and MSI results keep the same variation trends as the incidence angles increase. 3) Generally, the interaction effects among parameters in the L-MEB model are increased as the incidence angles increase, especially for the parameters of N_R and *SM* in the V-pol conditions, which can be clearly observed in Fig. 2(c) and (f). As a result, the following analyses are simply based on the TSI values for the completeness of the sensitivity index consideration.

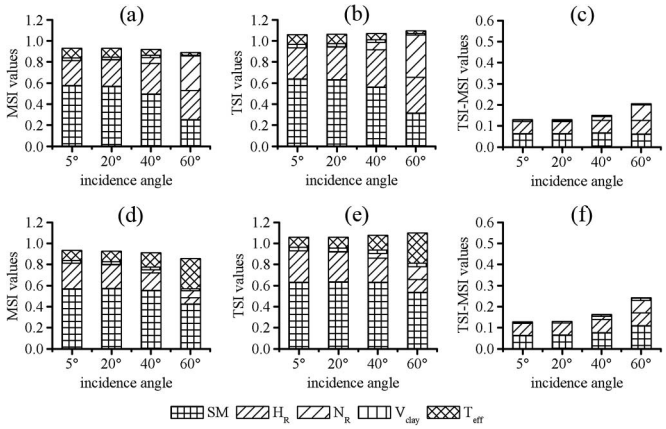

Fig. 2. MSI, TSI, and their difference values of all parameters in the L-MEB model for bare soils. (a)–(c) For H-pol conditions. (d)–(f) For V-pol conditions.

Meanwhile, the physical correctness of the global SA method of eFAST is specially validated in Figs. 3 and 4 through the property at the Brewster angle (around 70°). Fig. 3(a) simulates the H-pol and V-pol brightness temperature from the L-MEB model at different soil moisture conditions and for different incidence angles of 20°, 40°, 60°, and 70°. Fig. 3(b) then gives the local SA results of *TB* to *SM* based on Fig. 3(a). Fig. 4 conducts an analogous global SA based on the eFAST method with the specific soil moisture condition of 0.2 $\mathrm{cm}^3/\mathrm{cm}^3$ and clay content of 30%. It can be clearly observed in Fig. 3(b) that, for v-pol conditions, the local *SM* sensitivity becomes around 0 when *SM* is between 0.15 and 0.2 $\mathrm{cm}^3/\mathrm{cm}^3$ at the incidence angle of 70°. The global sensitivity results in Fig. 4 also show that, around the Brewster angle (70°), the V-pol L-MEB model results are sensitive to nothing but the parameter of T_{eff} at the soil moisture condition of 0.2 $\mathrm{cm}^3/\mathrm{cm}^3$. All of these results go in accordance with the property at the Brewster angle when the specular reflectivity of the soil surface is 0. They are used to prove the physical correctness of the eFAST analysis results.

As the global SA results show in Fig. 2 and Table II, *SM*, H_R, and T_{eff} are the three most sensitive factors for bare soils at the incidence angles of 5°–40°, with the TSI values of about 0.5–0.6, 0.2–0.4, and 0.1–0.2, respectively. The sensitivities of V_{clay} and N_R are much lower than those of *SM*, H_R, and T_{eff}, with the TSI values of about 0–0.1. However, at the incidence angle of 60°, the sensitivity of N_R increases significantly for H polarization, and the sensitivity of T_{eff} increases greatly for V polarization. This indicates that, at the extreme high incidence angles, the incidence-related adjust parameters, such as N_R, will severely affect the H-pol model results, while the V-pol simulations are more sensitive to temperature-related parameters.

TABLE II
eFAST SENSITIVITY RESULTS OF ALL PARAMETERS IN THE L-MEB MODEL FOR BARE SOILS. (a) MSI VALUES OF ALL THE PARAMETERS FOR THE BARE SOILS. (b) TSI VALUES OF ALL THE PARAMETERS FOR THE BARE SOILS

(a)

Input Para.	H-pol				V-pol			
	5°	20°	40°	60°	5°	20°	40°	60°
SM	0.58	0.57	0.49	0.25	0.57	0.57	0.56	0.43
H_R	0.24	0.25	0.29	0.28	0.24	0.23	0.16	0.06
N_R	0.00	0.00	0.05	0.33	0.00	0.00	0.03	0.07
V_{clay}	0.03	0.03	0.02	0.01	0.03	0.03	0.02	0.02
T_{eff}	0.09	0.08	0.06	0.02	0.10	0.10	0.14	0.29
Total	**0.93**	**0.93**	**0.92**	**0.89**	**0.93**	**0.93**	**0.91**	**0.86**

(b)

Input Para.	H-pol				V-pol			
	5°	20°	40°	60°	5°	20°	40°	60°
SM	0.64	0.63	0.56	0.31	0.63	0.64	0.63	0.54
H_R	0.29	0.31	0.35	0.34	0.30	0.28	0.23	0.12
N_R	0.00	0.00	0.07	0.40	0.00	0.00	0.05	0.12
V_{clay}	0.03	0.03	0.03	0.01	0.03	0.03	0.03	0.03
T_{eff}	0.09	0.09	0.06	0.03	0.10	0.10	0.14	0.29
Total	**1.06**	**1.06**	**1.07**	**1.10**	**1.06**	**1.06**	**1.08**	**1.10**

TABLE III
eFAST SENSITIVITY RESULTS OF ALL PARAMETERS IN THE L-MEB MODEL FOR VEGETATION COVERS. (a) MSI VALUES OF ALL THE PARAMETERS FOR THE VEGETATION COVERS. (b) TSI VALUES OF ALL THE PARAMETERS FOR THE VEGETATION COVERS

(a)

Input Para.	H-pol				V-pol			
	5°	20°	40°	60°	5°	20°	40°	60°
SM	0.42	0.31	0.12	0.03	0.41	0.31	0.13	0.02
H_R	0.17	0.14	0.07	0.03	0.17	0.12	0.04	0.00
N_R	0.00	0.00	0.01	0.03	0.00	0.00	0.01	0.00
V_{clay}	0.02	0.01	0.00	0.00	0.02	0.01	0.01	0.00
T_{eff}	0.19	0.20	0.19	0.17	0.19	0.24	0.39	0.62
τ_{NAD}	0.10	0.17	0.27	0.32	0.10	0.14	0.11	0.01
tt	0.00	0.01	0.05	0.05	0.00	0.01	0.01	0.00
ω	0.01	0.02	0.04	0.06	0.01	0.02	0.07	0.18
Total	**0.90**	**0.86**	**0.76**	**0.68**	**0.90**	**0.86**	**0.76**	**0.84**

(b)

Input Para.	H-pol				V-pol			
	5°	20°	40°	60°	5°	20°	40°	60°
SM	0.50	0.41	0.24	0.11	0.49	0.41	0.27	0.08
H_R	0.23	0.20	0.16	0.14	0.23	0.18	0.10	0.02
N_R	0.00	0.00	0.03	0.13	0.00	0.00	0.02	0.02
V_{clay}	0.02	0.02	0.01	0.02	0.02	0.02	0.01	0.01
T_{eff}	0.19	0.20	0.19	0.18	0.19	0.25	0.39	0.62
τ_{NAD}	0.16	0.27	0.46	0.61	0.16	0.25	0.29	0.12
tt	0.00	0.02	0.09	0.15	0.00	0.02	0.05	0.03
ω	0.01	0.02	0.05	0.09	0.01	0.02	0.08	0.21
Total	**1.11**	**1.16**	**1.24**	**1.43**	**1.11**	**1.15**	**1.22**	**1.12**

Other incidence-related results can also be observed in Fig. 2: 1) an obviously decreasing *SM* sensitivity with increasing incidence angle is found for both the H-pol and V-pol simulation results, although the decreasing trend is much weakened for the V-pol simulations and is disturbed by the tiny higher TSI values at the incidence angle of 20°; 2) another finding about

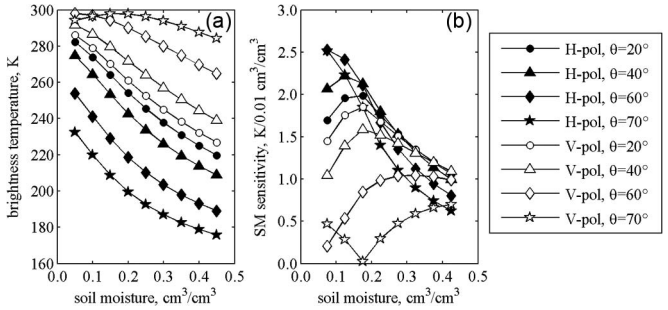

Fig. 3. (a) Forward simulated L-MEB model results and (b) local *SM* SA results with different soil moisture and different incidence angles.

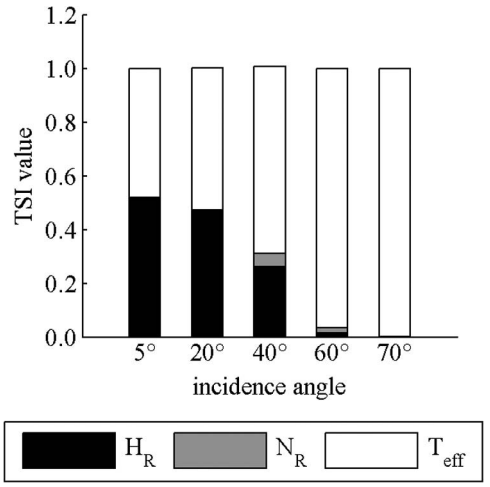

Fig. 4. Global SA results of the L-MEB model parameters when $\mathrm{SM} = 0.2\ \mathrm{cm}^3/\mathrm{cm}^3$ and $V_{\mathrm{clay}} = 30\%$ for different incidence angles and V-pol conditions.

the *SM* sensitivities in Fig. 2 is that the obviously higher *SM* sensitivity for the V-pol conditions than that for the H-pol conditions is found at the larger incidence angles of 40° and 60°; and 3) for the other parameters of H_R and T_{eff}, the just opposite sensitivity variation trends with increasing incidence angle are found for both H-pol and V-pol simulations. It indicates that the V-pol model results are more sensitive to temperatures, resulting in their less sensitivity to roughness-related parameters comparing with that in the H-pol cases.

However, some of these results are different from the traditional SA results of the L-MEB model, as shown in Fig. 5 (take the parameter *SM* for example, when $N_R = 0$): 1) the H-pol *SM* sensitivity is consistently larger than that for the V-pol conditions; 2) a slightly increasing *SM* sensitivity with increasing incidence angle in H-pol simulations; and 3) a decreasing *SM* sensitivity under the V-pol conditions. These differences can be partially explained by the different implications of sensitivity in the local and global SA methods. Traditionally, the local SA method is gradient-based, and it analyzes one parameter in a model each time by holding all of the other parameters fixed. As a result, the local sensitivities are absolute and with their unique units, which cannot be compared among parameters. Moreover, the local sensitivity values are always unfixed, conditionally on the settings of other parameter values. The situation is clearly demonstrated in Fig. 5 when $N_R \neq 0$ is set so that the results

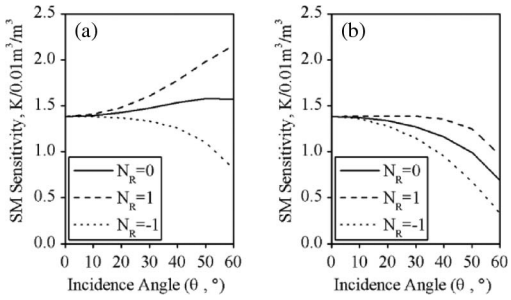

Fig. 5. *SM* sensitivities to the L-MEB model at different incidence angles with the traditional local SA method. (a) and (b) For H and V polarizations, respectively.

are quite different from those when $N_R = 0$ is used. While in the global SAs, such as the eFAST, all of the parameters in a model can be analyzed at one time. Their sensitivities are calculated based on the idea of variation decomposition so that the results are correlative with each other with the total sensitivities of all parameters summing to around 1 in general. Hence, the sensitivity of a parameter in the global SAs is dimensionless and is actually the relative importance of that parameter compared with other parameters in one model. Meanwhile, the global sensitivity values are stable as long as the parameters and their values ranges are given in the analyses. As a result, the global sensitivities can be compared with each other in one experiment or in different analogous experiments concerning their relative importance, rather than the absolute amounts in different and incomparable units, which makes the main advantage of the global SA methods. To conclude, the different sensitivity results in Figs. 2 and 5 maybe lie in the different interpretations of sensitivity in their definitions, which cannot be directly compared in applications. The global sensitivities will be conducted in more and more applications in all fields in the future.

To sum up, the sensitivity results in this global analysis are quite different from those found from the traditional local analyses, which can be explained by the different interpretations of sensitivity in the global and local SA methods. According to the global analyses, *SM*, H_R, and T_{eff} make the three most sensitive parameters in the L-MEB model for bare soils, with the exception when the extremely high incidence angles are taken. It proves the retrievability of *SM* and H_R for bare soils in the traditional multiparameter retrieval methods. The results also emphasize the sensitivity of T_{eff}, especially for V-pol conditions at the higher incidence angles, making it another choice to be considered in the future multiparameter retrieval combinations. As the incidence angle increases, the V-pol model results are more sensitive to the temperature parameters, while the H-pol model simulations are more sensitive to the roughness-related parameters.

2) Test 1 for Vegetation Covers: The comparison between the MSI and TSI values for vegetation covers is similar to that for bare soils in the aforementioned section, with the main differences that the interaction effects among parameters in the L-MEB model for vegetation covers are much stronger than those for bare soils, which can be observed in Fig. 6(c) and (f). However, the interaction effects are still not altered

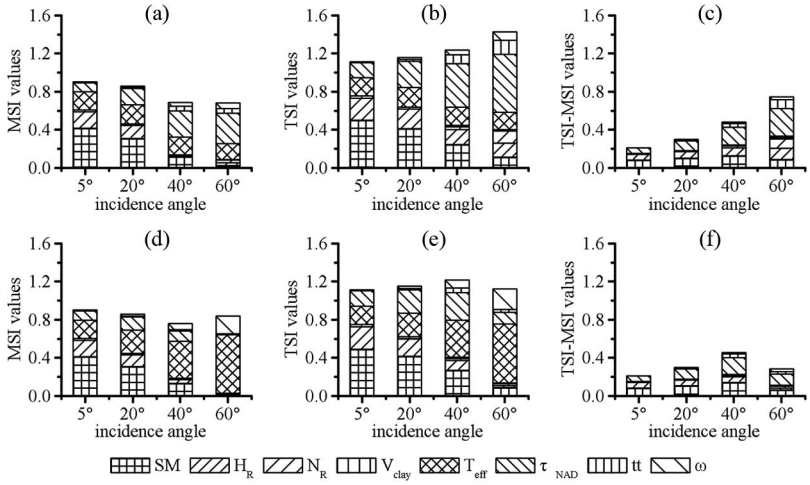

Fig. 6. MSI, TSI, and their difference values of all parameters in the L-MEB model for vegetation covers. (a)–(c) For H-pol conditions. (d)–(f) For V-pol conditions.

associated with the sensitivity variation trends of TSI and MSI with the increasing incidence angles, and the following analyses are then also based on one sensitivity index of TSI in Fig. 6(b) and (e).

For vegetation covers, as shown in Fig. 6(b) and (e), *SM*, H_R, $\tau_{\rm NAD}$, and $T_{\rm eff}$ are the four most sensitive factors in the L-MEB model for vegetation covers, with the TSI values varying between about 0.1 and 0.6 individually. Note that their rankings vary at different incidence angles. At low incidence angles of 5° and 20°, the most sensitive parameter is *SM*, with the TSI values being about 0.4–0.5; the remaining three parameters of $\tau_{\rm NAD}$, $T_{\rm eff}$, and H_R are with sensitivity values of about 0.1–0.3. However, at high incidence angles of 40° and 60°, the parameters $\tau_{\rm NAD}$ and $T_{\rm eff}$ become the two most sensitive factors, with the most sensitive parameter being $\tau_{\rm NAD}$ for H polarization and $T_{\rm eff}$ for V polarization. In particular, compared with the sensitivities at the incidence angles 5° and 20°, the sensitivity values of the other two parameters of *SM* and H_R are significantly decreased, with the low TSI values of about 0–0.3. Other parameters N_R, tt, ω, and $V_{\rm clay}$ have relatively low TSI values, varying between about 0–0.2, and an increasing sensitivity trend with increased incidence angle is found for all of these parameters, but $V_{\rm clay}$.

Other incidence-related results that can be observed in Fig. 6(b) and (e) include the following: 1) both the sensitivities of *SM* and H_R decrease as the incidence angle increases, and 2) a general increasing sensitivity trend for both $\tau_{\rm NAD}$ and $T_{\rm eff}$ is observed for both H and V-pol conditions except for the slightly decreasing $T_{\rm eff}$ sensitivity in H-pol conditions and the decreasing $\tau_{\rm NAD}$ sensitivity at the extreme high incidence angle of 60° under V-pol conditions. Similar to the behaviors for bare soils in Fig. 4 ($\theta = 70°$), the abnormal behavior of sensitivity results under V-pol and $\theta = 60°$ conditions can be partially attributed to what occurs around the Brewster angle when the TSI values of $T_{\rm eff}$ are extremely high. Some of these results are different from those for bare soils, mainly observed in H-pol conditions for H_R. The decreasing H-pol sensitivity of H_R for vegetated soils is together with the drastically increasing sensitivity of $\tau_{\rm NAD}$, which can be explained by the radiative transfer process theoretically: as the incidence angle increases, the path length radiation traveling through the vegetation increases, resulting to the increasing influences of vegetation on the model results and the decreasing influences of the soil emission. As a result, the sensitivity increases with θ for the vegetation-related parameters like $\tau_{\rm NAD}$, tt, and ω, while the sensitivities decrease for the soil-related parameters such as *SM* and H_R.

As the conclusion, *SM*, H_R, $\tau_{\rm NAD}$, and $T_{\rm eff}$ are the four most sensitive parameters in the L-MEB model for vegetated covers, proving their retrievability in the past and future multiparameter retrieval methods. Additionally, like the situations for bare soils, the V-pol model results are more sensitive to temperature parameters, while the H-pol model simulations are more sensitive to the vegetation and roughness parameters, especially for the higher incidence angles.

B. Test 2: Parameters' Sensitivity Variation Analysis

In this test, all parameters but H_R or $\tau_{\rm NAD}$ are included in the eFAST method, and their TSI values are analyzed under different roughness or vegetation conditions. The effects of $T_{\rm eff}$ are specially considered by setting constant $T_{\rm eff}$ values in the analogous analyses. Like the explanation in test 1, the TSI values also indicate the feasibility of each parameter to be retrieved in the inversion, and the TSI variations then reflect the stability of their retrievability under different land surface conditions. Due to the different influences of vegetation and roughness at different incidence angles, the analyses are based on the data acquired at two specific incidence angles of 5° and 40°, and in the following figures, only the H-pol results for 5° are kept in order to save space as the sensitivity results at the low incidence angles are almost the same for both H-pol and V-pol conditions.

1) Test 2 for Bare Soils: For bare soils, the variations of the TSI values for all parameters but H_R under different roughness conditions are shown in Fig. 7(a)–(c), with subplots (a) for H-pol and the incidence angle of 5°, (b) for H-pol and $\theta = 40°$, and (c) for V-pol and $\theta = 40°$. The effects of $T_{\rm eff}$ are particularly considered in Fig. 7(d)–(f), with subplots (d) for H-pol and $\theta = 5°$, (e) for H-pol and $\theta = 40°$, and (f) for V-pol and $\theta = 40°$. The last three subplots are specially obtained

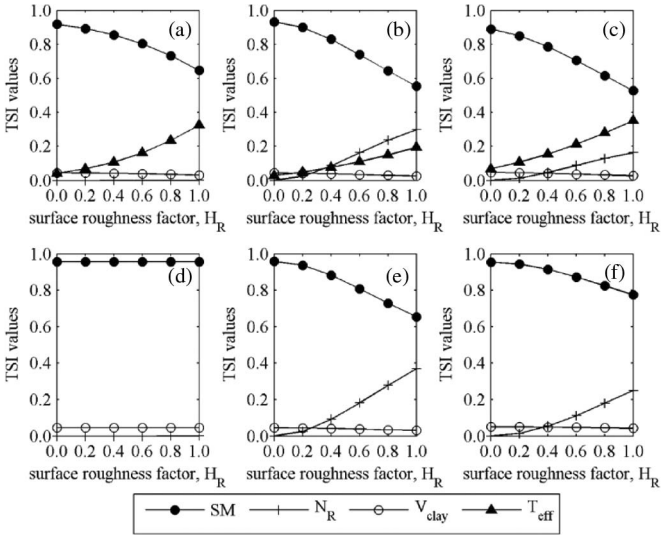

Fig. 7. TSI variations of all parameters but H_R for bare soils under different roughness conditions, with a variable $T_{\rm eff}$ of 0 °C–40 °C in (a), (b), and (c) and a fixed $T_{\rm eff}$ of 25 °C in (d), (e), and (f). (a) and (d) For $\theta = 5°$, H-pol. (b) and (e) For $\theta = 40°$, H-pol. (c) and (f) For $\theta = 40°$, V-pol conditions.

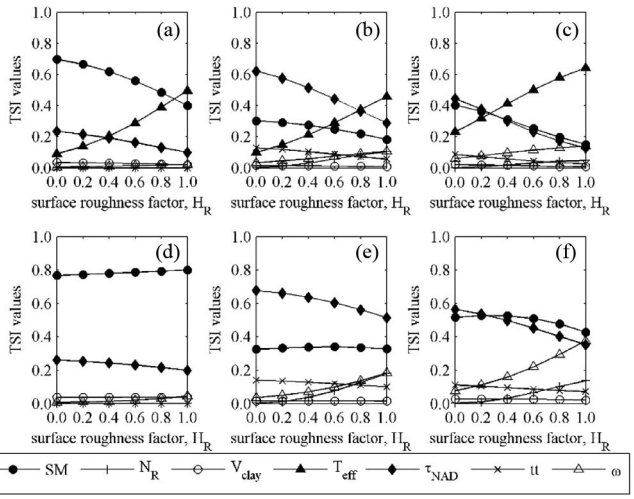

Fig. 8. TSI variations of all parameters but H_R for vegetation covers under different roughness conditions, with a variable $T_{\rm eff}$ of 0 °C–40 °C in (a), (b), and (c) and a fixed $T_{\rm eff}$ of 25 °C in (d), (e) and (f). (a) and (d) For $\theta = 5°$, H-pol. (b) and (e) For $\theta = 40°$, H-pol. (c) and (f) For $\theta = 40°$, V-pol conditions.

to discuss the sensitivity variations with H_R with the default constant $T_{\rm eff}$ value of 25 °C in Table I. Essentially, Fig. 7 is similar to Fig. 2 except for the different number of input L-MEB model parameters explored by the eFAST method. All of the findings are listed in the following.

First, the decreasing *SM* sensitivity from about 0.9–0.4 and consistently increasing $T_{\rm eff}$ sensitivity from about 0.1–0.5 are observed in the first three subplots of Fig. 7, which indicate that, in the traditional "3-P" method for bare soils, the *SM* retrievability is decreasing independent of incidence angle and polarization as the land surface becomes rougher, corresponding to the obviously increasing $T_{\rm eff}$ sensitivity to the forward L-MEB model results. Then, the analogous experiments in Fig. 7(d)–(f) with the known $T_{\rm eff}$ value of 25 °C show that, comparing to the decreasing *SM* sensitivity with H_R in Fig. 7(a)–(c), the decreasing trend in Fig. 7(a) has almost disappeared when $T_{\rm eff}$ is given in Fig. 7(d) when $\theta = 5°$, and the decreasing trend in Fig. 7(b) and (c) is much mitigated in Fig. 7(e) and (f) when $\theta = 40°$. This means that, in the traditional "3-P" method for bare soils, the *SM* retrievability will be consistently high as long as accurate input $T_{\rm eff}$ data are provided.

Second, there is an increasing N_R sensitivity in Fig. 7(b) and (c) for $\theta = 40°$, which aggravates the decreasing rate of the *SM* sensitivity, especially for the H-pol conditions in Fig. 7(b). The increasing N_R sensitivity with H_R is also observed in Fig. 7(e) and (f) when the $T_{\rm eff}$ value is known. All of these findings indicate that the input error of the parameter N_R would be another important error resource in the *SM* retrieval under rough surface conditions, especially for the larger incidence angle conditions. Finally, the TSI values of $V_{\rm clay}$ are consistently low in all subplots of Fig. 7, being around 0.05 and with a slightly decreasing trend to about 0.02 as the surface roughness increases, which means that, in the forward L-MEB model, even if the underlying soil model may not correctly simulate the effect of clay content on the soil dielectric constant, the impact of the clay content error on the model results will be low. This then indicates the consistently low possibility of $V_{\rm clay}$ to be the error resource in the multiparameter retrievals under different land roughness conditions.

To sum up, the aforementioned findings emphasize the first importance of high-precision surface temperature data to be provided in the traditional "3-P" approach when the lands become rougher for bare soils. Additionally, an accurate N_R value is also needed to guarantee the accurate *SM* retrievals under rough surface conditions and at the large incidence angles.

2) Test 2 for Vegetation Covers: For vegetation covers, the variations of the TSI values for all parameters but H_R are shown in Fig. 8(a)–(c) under different roughness conditions, and the analogous sensitivity variations with H_R are then conducted in (d), (e), and (f) with the constant $T_{\rm eff}$ value of 25 °C. Fig. 9 summarizes the variations of TSI values for all parameters but $\tau_{\rm NAD}$ for different vegetation conditions in the first three subplots, and the effects of $T_{\rm eff}$ are particularly considered in the other three subplots of (d), (e), and (f). In both figures, subplots (a) and (d) are for H-pol and $\theta = 5°$, (b) and (e) for H-pol and $\theta = 40°$, and (c) and (f) for V-pol and $\theta = 40°$. Similar to that for bare soils, Figs. 8 and 9 are similar to Fig. 6 except for the different numbers and the combinations of the input L-MEB model parameter explored by the eFAST method. All of the findings are listed in the following.

Similar to the cases for bare soils, the most evident findings in Figs. 8 and 9 are that the sensitivities of *SM* and $\tau_{\rm NAD}$ decrease consistently, while the $T_{\rm eff}$ sensitivity increases greatly as the land roughness increases as shown in Fig. 8(a)–(c); the sensitivities of *SM* and H_R decease consistently, while the $T_{\rm eff}$ sensitivity increases greatly as the vegetation becomes denser as revealed in Fig. 9(a)–(c). In particular, the $T_{\rm eff}$ sensitivity is extremely high for rougher and more vegetated lands in (b) and (c) of Figs. 8 and 9 at the incidence angle of 40°, resulting to the very low sensitivities of *SM* and $H_R/\tau_{\rm NAD}$. The results similarly suggest the decreasing retrievability of *SM* in the traditional "3-P" method when the land is rougher or the

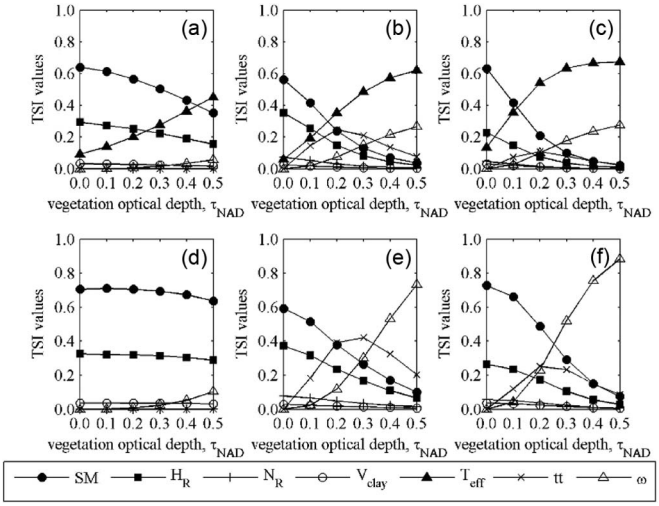

Fig. 9. TSI variations of all parameters but $\tau_{\rm NAD}$ for vegetation covers under different vegetation conditions, with a variable $T_{\rm eff}$ of 0 °C–40 °C in (a), (b), and (c) and a fixed $T_{\rm eff}$ of 25 °C in (d), (e) and (f). (a) and (d) For $\theta = 5°$, H-pol. (b) and (e) For $\theta = 40°$, H-pol. (c) and (f) For $\theta = 40°$, V-pol conditions.

vegetation is denser. In both figures, the decreasing *SM* and $\tau_{\rm NAD}/H_R$ sensitivities in (a), (b), and (c) are greatly improved in (d), (e), and (f) when the $T_{\rm eff}$ value is known, which indicates the improved retrievability of these parameters with known $T_{\rm eff}$ values in the retrievals.

Other parameters like tt, N_R, and $V_{\rm clay}$ usually have consistently low TSI values under different roughness and vegetation conditions, except for the parameter of tt in Fig. 9(b) and (c) for a large incidence angle of 40°. The unusual variation trend of first increasing and then decreasing tt sensitivity with $\tau_{\rm NAD}$ in Fig. 9(b) and (c) is explainable, considering the fact that the vegetation structure effect will decline when the vegetation is dense enough. The parabolic variation trend of tt sensitivities with $\tau_{\rm NAD}$ is more obvious in Fig. 9(e) and (f) for the larger incidence angle of 40° when the $T_{\rm eff}$ sensitivity is eliminated. All of these findings indicate the increased effect of tt on the model results and the retrieval results for lands with medium vegetation covers at the larger incidence angles, and the effects will be further increased when the $T_{\rm eff}$ values are known during the simulations or retrievals.

Finally, a low but gradually increasing trend of ω sensitivity is observed in both Figs. 8 and 9 for the larger incidence angle of 40° in subplots (b) and (c). This increasing trend is more obvious in the analogous subplots of (e) and (f) when the $T_{\rm eff}$ values are known, which indicate that, besides the parameters of $T_{\rm eff}$ and tt, the accuracy of ω would also affect the simulations and retrievals greatly when the vegetation grows denser, mainly for larger incidence angles and especially for simulations and retrievals with known $T_{\rm eff}$ values.

The results similarly suggest the decreasing retrievability of *SM* in the traditional "3-P" method when the land is rougher or the vegetation is denser, which can be partially improved by employing the high-precision surface temperature data in the multiparameter retrievals. From the perspective of algorithm improvement, this also means that it would be an effective choice to include the parameter of $T_{\rm eff}$ into the combination

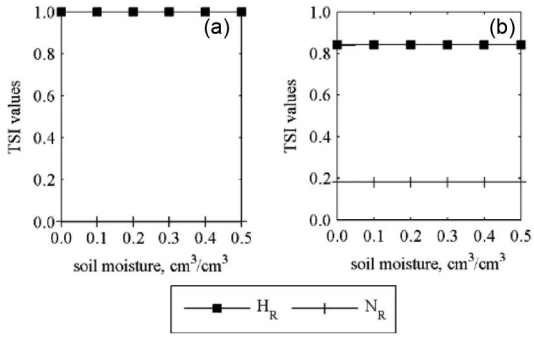

Fig. 10. TSI variations of the calibrating parameters under different soil moisture conditions for bare soils. (a) $\theta = 5°$ for H polarization. (b) $\theta = 40°$ for H polarization.

of the retrieval parameters in the new multiparameter retrieval methods. For the empirical parameters, the parameters ω and tt affect the model results more than any other parameters, calling for the needs of accurate calibration results to be provided before the retrievals.

V. Test 3: Calibration Parameters Included Only

The parameters to be calibrated in the L-MEB model include the roughness-related parameters H_R, $N_{\rm RH}$, and $N_{\rm RV}$ only for bare soils; for vegetation covers, other vegetation-related parameters including $\tau_{\rm NAD}$, tt_H, tt_V, ω_H, and ω_V also need to be calibrated before the retrieval processes.

The traditional calibration method means the retrieval of the calibrating parameters based on the given *TB* and *SM* observations in nature. In this test, the sensitivity of the calibration parameters is analyzed under different soil moisture conditions as shown in Figs. 10 and 11, and the other parameters are set as follows: $T_{\rm eff} = 25$ °C and $V_{\rm clay} = 30\%$ given in Table I. The TSI values here also represent the sensitivity of the modeled *TB* values to the variation of each input parameter, and the higher TSI values indicate the higher possibility of that parameter to be calibrated as a result.

1) Test 3 for Bare Soils: In Fig. 10, the TSI variations of the calibrated parameters with different soil moisture are compared at two incidence angles 5° and 40°. Only the results in H polarization are shown because the results are similar for both H and V polarizations.

It is shown in Fig. 10 that, at small incidence angles, the sensitivity of $\mathtt{H}_R$ is close to 1, and the sensitivity of N_R approaches 0 for all soil moisture conditions. At larger incidence angles, the sensitivity of H_R declines to about 0.8, and the sensitivity of N_R increases to about 0.2. The high sensitivities of H_R indicate the high capability of the parameter to be calibrated for bare soils, and the capability of N_R to be calibrated is evident only at large incidence angles.

It can also be seen in Fig. 10 that the TSI variations of H_R and N_R with soil moisture are insignificant, indicating the high stability of the calibration results under different soil moisture conditions. Relatively consistent results can then be obtained based on different soil moisture observations in the calibrations.

2) Test 3 for Vegetation Covers: For vegetation covers, the TSI variations of the calibrated parameters with different soil

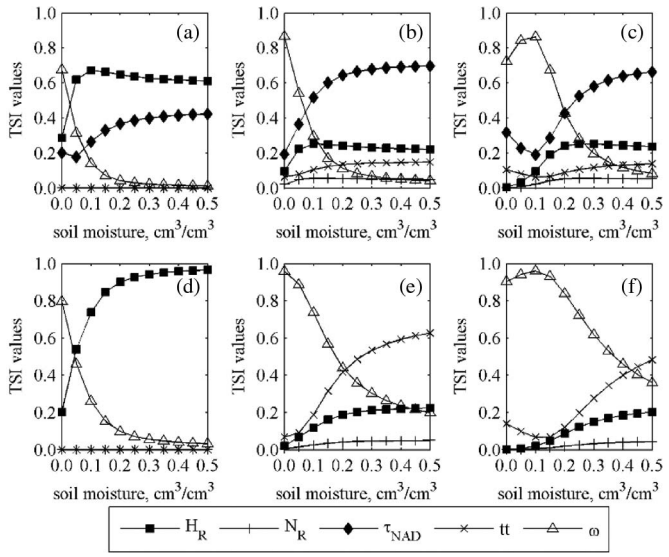

Fig. 11. TSI variations of the calibrating parameters under different soil moisture conditions for vegetation covers, with a variable τ_{NAD} of 0–0.5 in (a), (b), and (c) and a fixed τ_{NAD} of 0.3 in (d), (e), and (f). (a) and (d) For $\theta = 5^\circ$, H-pol. (b) and (e) For $\theta = 40^\circ$, H-pol. (c) and (f) For $\theta = 40^\circ$, V-pol conditions.

moisture in both H and V polarizations are compared at two incidence angles 5° and 40° in Fig. 11(a)–(c), with subplots (a) for H-pol and $\theta = 5^\circ$, (b) for H-pol and $\theta = 40^\circ$, and (c) for V-pol and $\theta = 40^\circ$. The case of V-pol and $\theta = 5^\circ$ is omitted as it is almost the same as that for H-pol condition. An analogous experiment is additionally performed in Fig. 11(d)–(f) to discuss the sensitivity variation of the other calibrated parameters when the amount of vegetation is known. This experiment represents an idealized version of what is attempted, for example, by the SMAP mission where ancillary data are used to determine the amount of vegetation before a soil moisture retrieval is made [17]. Fig. 11(d)–(f) is similar to Fig. 11(a)–(c), except for the constant τ_{NAD} value of 0.3 given in Table I.

It is shown in Fig. 11(a)–(c) that the parameters of H_R, τ_{NAD}, and ω are the three most sensitive factors in the calibration, but their TSI values vary a lot under different soil moisture conditions. When the land is dry, the parameter ω is the primary sensitive factor with extremely high TSI values. However, its TSI values drop rapidly to a low and relatively consistent level when the soil moisture is increased to about 0.10 m^3/m^3 at low incidence angles and about 0.20 m^3/m^3 at high incidence angles. For moist land, H_R and τ_{NAD} become the first two most sensitive factors in the calibration, with relatively consistent TSI values of about 0.6 and 0.2 for H_R and slightly increasing TSI values between about 0.3–0.4 and 0.5–0.7 for τ_{NAD} at two different incidence angles. The sensitivities of tt and N_R are very small at low incidence angles, with TSI values of about 0–0.05, and the values increase to about 0.1–0.2 at large incidence angles, indicating bad retrievability and potentially poor calibration results of these parameters in the current calibration method.

When the amount of vegetation is known, like the case in Fig. 11(d)–(f) for medium vegetation coverage with $\tau_{\mathrm{NAD}} = 0.3$, the most sensitive parameters in the calibration vary a lot for different incidence angles. H_R is the dominant sensitive factor when the soils are wet at the low incidence angle 5°, while ω and tt are the two main sensitive factors at the large incidence angle 40°, with ω being more dominant for dry soils and tt for wet soils. This indicates the potentially high retrievability of H_R at low incidence angles and good retrievability of ω and tt at higher incidence angles, although the reliability of the retrievals depends greatly on the soil moisture condition. A more straightforward finding is that much higher TSI values for the parameters of H_R in Fig. 11(d) and the relatively higher TSI values of ω and tt in Fig. 11(e) and (f) are observed with known vegetation information, which indicates better retrievability of these parameters compared with that when the amount of vegetation is unknown as shown in Fig. 11(a)–(c).

As a result, for unknown τ_{NAD} conditions, the following can be concluded from the aforementioned findings: 1) a satisfactory calibration result can be only found for the parameters of τ_{NAD} and H_R, and only when the soils are moist enough. 2) For dry soil conditions, the potentially poor results in calibrating τ_{NAD} and H_R are related to the extremely high but decreasing sensitivity of ω. One possible explanation is that the vegetation effect, referring to the attenuation effect here, will exceed the effect of soil emission and the vegetation emission in the L-MEB model when the land is dry enough. However, in reality, the soils are usually moist for vegetated land, especially for croplands and alpine grasslands, supporting the current calibration method in calibrating τ_{NAD} and H_R. 3) For the other semiempirical parameters ω, tt, and N_R, the current calibration method may be not suitable to calibrate them, considering their low or inconsistent sensitivity values in the eFAST method. For the future development of the current calibration method, some different findings are found when the amount of vegetation is known in the calibration. For example, the incidence angles affect the calibration results greatly, with potentially good calibration results of H_R at low incidence angles and better calibration results of ω and tt at larger incidence angles. Furthermore, the reliability of the calibration results depends largely on the soil moisture condition, and the retrievabilty is much improved compared with the unknown amount of vegetation conditions.

VI. Conclusion

In this paper, a variance-based SA has been used to conduct a parameter SA of the L-MEB model. Three different SA tests are designed. The global sensitivity results are found to be quite different from those found in traditional local analyses. The differences are explained, and the results are analyzed to direct the applications of the L-MEB model in parameter calibrations and surface parameter retrievals.

The eFAST method was used to conduct this analysis. It is helpful in studying the reliability and the potential improvements to the current multiparameter retrieval methods. Surface soil moisture, soil roughness factor, vegetation optical depth at nadir, and effective land surface temperature are the four main sensitivity parameters in the L-MEB model. The results prove the retrievability of the first three parameters in the traditional "3-P" retrieval method and provide a new choice to include

the effective land surface temperature in the combination of the retrieval parameters in the future multiparameter retrievals. The sensitivity variation analysis of these parameters under different surface roughness and vegetation conditions also emphasizes the importance of effective land surface temperature, considering it imperative to have high-precision land surface temperature data provided to guarantee the accurate soil moisture retrievals in the traditional "3-P" retrieval method when the lands become rougher or more vegetated. Another interesting finding is that the V-pol global sensitivities of soil moisture are always higher than those for the H-pol conditions at the high incidence angles. The results are just opposite from many other researches using the traditionally gradient-based analysis methods. Such difference indicates that there is a need to conduct further studies to give the explanations in the future.

The eFAST method is also valuable in discussing the current calibration methods. A satisfactory calibration result for the parameters of soil roughness factor and vegetation optical depth at nadir may be achieved when the amount of vegetation is unknown. However, the very low or inconsistent sensitivity of the other parameters of vegetation structure factor, single scattering albedo, and soil roughness coefficient indicates the possibly poor calibration results of these parameters. Consequently, new calibration procedures that account for the different relative sensitivities of these model parameters at higher incidence angles or different soil moisture conditions may need to be developed in the future. Other calibration methods based on the physical model simulations or more observations are also needed to be considered. One improved calibration method with known vegetation amount has shown better retrievability of the calibrated parameters, although their retrievabilities vary greatly with incidence angle and soil moisture.

The aforementioned strategy of discussing the feasibility of a model and its effect based on a quantitative sensitive analysis method like the eFAST method can also be used for the other multiparameter models. However, several caveats should be noted: the analysis is based on the mathematical statistics of the model, and the correctness of the results depends on the theoretical foundation of the model. Furthermore, the discussions about the application effects of a model are more instructive rather than determinative, and more field experiment data are still needed to verify or overthrow these discoveries.

ACKNOWLEDGMENT

The authors would like to thank Dr. J.-P. Wigneron for kindly providing the L-MEB model and acknowledge the assistance of Dr. S. Tarantola for the suggestions on the eFAST method.

REFERENCES

[1] Y.-A. Liou and A. W. England, "A land-surface process/radiobrightness model with coupled heat and moisture transport for freezing soils," *IEEE Trans. Geosci. Remote Sens.*, vol. 36, no. 2, pp. 669–677, Mar. 1998.

[2] Y.-A. Liou and A. W. England, "A land surface process/radiobrightness model with coupled heat and moisture transport in soil," *IEEE Trans. Geosci. Remote Sens.*, vol. 36, no. 1, pp. 273–286, Jan. 1998.

[3] Y. H. Kerr, "Soil moisture from space: Where are we?" *Hydrogeol. J.*, vol. 15, no. 1, pp. 117–120, Feb. 2007.

[4] T.-Y. Chang, Y.-A. Liou, C.-Y. Lin, S.-C. Liu, and Y.-C. Wang, "Evaluation of surface heat fluxes in Chiayi plain of Taiwan by remotely sensed data," *Int. J. Remote Sens.*, vol. 31, no. 14, pp. 3885–3898, Aug. 2010.

[5] T.-Y. Chang *et al.*, "Estimation of root zone soil moisture using apparent thermal inertia with MODIS imagery over a tropical catchment in Northern Thailand," *IEEE J. Sel. Topics Appl. Earth Observ. Remote Sens.*, vol. 5, no. 3, pp. 752–761, Jun. 2012.

[6] T. Schmugge, P. E. O'Neill, and J. R. Wang, "Passive microwave soil moisture research," *IEEE Trans. Geosci. Remote Sens.*, vol. GE-24, no. 1, pp. 12–22, Jan. 1986.

[7] E. G. Njoku, Y. Rahmat-Samii, J. Sercel, W. J. Wilson, and M. Moghaddam, "Evaluation of an inflatable antenna concept for micro wave sensing of soil moisture and ocean salinity," *IEEE Trans. Geosci. Remote Sens.*, vol. 37, no. 1, pp. 63–78, Jan. 1999.

[8] R. D. Magagi, Y. H. Kerr, and J.-C. Meunier, "Results of combining L- and C-band passive microwave airborne data over the Sahelian area," *IEEE Trans. Geosci. Remote Sens.*, vol. 38, no. 4, pp. 1997–2008, Jul. 2000.

[9] Y.-A. Liou, Y.-C. Tzeng, and K.-S. Chen, "A neural-network approach to radiometric sensing of land-surface parameters," *IEEE Trans. Geosci. Remote Sens.*, vol. 37, no. 6, pp. 2718–2724, Nov. 1999.

[10] Y.-A. Liou, K. Chen, and T.-D. Wu, "Reanalysis of L-band brightness predicted by the LSP/R model-for prairie grassland: Incorporation of rough surface scattering," *IEEE Trans. Geosci. Remote Sens.*, vol. 39, no. 1, pp. 129–135, Jan. 2001.

[11] S.-F. Liu, Y.-A. Liou, W.-J. Wang, J.-P. Wigneron, and J.-B. Lee, "Retrieval of crop biomass and soil moisture from measured 1.4 and 10.65 GHz brightness temperatures," *IEEE Trans. Geosci. Remote Sens.*, vol. 40, no. 6, pp. 1260–1268, Jun. 2002.

[12] Y.-A. Liou, S.-F. Liu, and W.-J. Wang, "Retrieving soil moisture from simulated brightness temperatures by a neural network," *IEEE Trans. Geosci. Remote Sens.*, vol. 39, no. 8, pp. 1662–1672, Aug. 2001.

[13] Y. H. Kerr *et al.*, "The SMOS mission: New tool for monitoring key elements of the global water cycle," *Proc. IEEE*, vol. 98, no. 5, pp. 666–687, May 2010.

[14] N. Djamai *et al.*, "Evaluation of SMOS soil moisture products over the CanEx-SM10 area," *J. Hydrol.*, vol. 520, pp. 254–267, Jan. 2015.

[15] S. Louvet *et al.*, "SMOS soil moisture product evaluation over West-Africa from local to regional scale," *Remote Sens. Environ.*, vol. 156, pp. 383–394, Jan. 2015.

[16] Y. H. Kerr *et al.*, "The SMOS soil moisture retrieval algorithm," *IEEE Trans. Geosci. Remote Sens.*, vol. 50, no. 5, pp. 1384–1403, May 2012.

[17] D. Entekhabi *et al.*, "The Soil Moisture Active Passive (SMAP) mission," *Proc. IEEE*, vol. 98, no. 5, pp. 704–716, May 2010.

[18] Y.-A. Liou and A. England, "Annual temperature and radiobrightness signatures for bare soils," *IEEE Trans. Geosci. Remote Sens.*, vol. 34, no. 4, pp. 981–990, Jul. 1996.

[19] Y.-A. Liou, E. Kim, and A. England, "Radiobrightness of prairie soil and grassland during dry-down simulations," *Radio Sci.*, vol. 33, no. 2, pp. 259–265, Mar./Apr. 1998.

[20] Y.-A. Liou, J. F. Galantowicz, and A. W. England, "A land surface process/radiobrightness model with coupled heat and moisture transport for prairie grassland," *IEEE Trans. Geosci. Remote Sens.*, vol. 37, no. 4, pp. 1848–1859, Jul. 1999.

[21] K.-S. Chen *et al.*, "Emission of rough surfaces calculated by the integral equation method with comparison to three-dimensional moment method simulations," *IEEE Trans. Geosci. Remote Sens.*, vol. 41, no. 1, pp. 90–101, Jan. 2003.

[22] S. Raju *et al.*, "Soil moisture and temperature profile effects on microwave emission at low frequencies," *Remote Sens. Environ.*, vol. 54, no. 2, pp. 85–97, Nov. 1995.

[23] K.-S. Chen, T.-D. Wu, M.-K. Tsay, and A. K. Fung, "Note on the multiple scattering in an IEM model," *IEEE Trans. Geosci. Remote Sens.*, vol. 38, no. 1, pp. 249–256, Jan. 2000.

[24] P. Xu, K. Chen, and L. Tsang, "Analysis of microwave emission of exponentially correlated rough soil surfaces from 1.4 GHz to 36.5 GHz," *Progr. Electromagn. Res.*, vol. 108, pp. 205–219, 2010.

[25] Y.-C. Wang, T.-Y. Chang, and Y.-A. Liou, "Terrain correction for increasing the evapotranspiration estimation accuracy in a mountainous watershed," *IEEE Geosci. Remote Sens. Lett.*, vol. 7, no. 2, pp. 352–356, Apr. 2010.

[26] J. Shi *et al.*, "A parameterized surface reflectivity model and estimation of bare-surface soil moisture with L-band radiometer," *IEEE Trans. Geosci. Remote Sens.*, vol. 40, no. 12, pp. 2674–2686, Dec. 2002.

[27] J. Shi *et al.*, "A parameterized multifrequency-polarization surface emission model," *IEEE Trans. Geosci. Remote Sens.*, vol. 43, no. 12, pp. 2831–2841, Dec. 2005.
[28] J. Shi *et al.*, "Physically based estimation of bare-surface soil moisture with the passive radiometers," *IEEE Trans. Geosci. Remote Sens.*, vol. 44, no. 11, pp. 3145–3153, Nov. 2006.
[29] T. R. Holmes, M. Drusch, J.-P. Wigneron, and R. A. de Jeu, "A global simulation of microwave emission: Error structures based on output from ECMWF's operational Integrated Forecast System," *IEEE Trans. Geosci. Remote Sens.*, vol. 46, no. 3, pp. 846–856, Mar. 2008.
[30] M. Owe, R. de Jeu, and J. Walker, "A methodology for surface soil moisture and vegetation optical depth retrieval using the microwave polarization difference index," *IEEE Trans. Geosci. Remote Sens.*, vol. 39, no. 8, pp. 1643–1654, Aug. 2001.
[31] J.-P. Wigneron *et al.*, "L-band microwave emission of the biosphere (L-MEB) model: Description and calibration against experimental data sets over crop fields," *Remote Sens. Environ.*, vol. 107, no. 4, pp. 639–655, Apr. 2007.
[32] J. R. Wang and B. Choudhury, "Remote sensing of soil moisture content, over bare field at 1.4 GHz frequency," *J. Geophys. Res.*, vol. 86, no. C6, pp. 5277–5282, Jun. 1981.
[33] C. Prigent, J.-P. Wigneron, W. B. Rossow, and J. R. Pardo-Carrion, "Frequency and angular variations of land surface microwave emissivities: Can we estimate SSM/T and AMSU emissivities from SSM/I emissivities?" *IEEE Trans. Geosci. Remote Sens.*, vol. 38, no. 5, pp. 2373–2386, Sep. 2000.
[34] K. Saleh *et al.*, "Estimates of surface soil moisture under grass covers using L-band radiometry," *Remote Sens. Environ.*, vol. 109, no. 1, pp. 42–53, Jul. 2007.
[35] J. P. Grant *et al.*, "Calibration of the L-MEB model over a coniferous and a deciduous forest," *IEEE Trans. Geosci. Remote Sens.*, vol. 46, no. 3, pp. 808–818, Mar. 2008.
[36] J.-P. Wigneron, L. Laguerre, and Y. H. Kerr, "A simple parameterization of the L-band microwave emission from rough agricultural soils," *IEEE Trans. Geosci. Remote Sens.*, vol. 39, no. 8, pp. 1697–1707, Aug. 2001.
[37] M. J. Escorihuela *et al.*, "A simple model of the bare soil microwave emission at L-band," *IEEE Trans. Geosci. Remote Sens.*, vol. 45, no. 7, pp. 1978–1987, Jul. 2007.
[38] J.-P. Wigneron *et al.*, "Evaluating an improved parameterization of the soil emission in L-MEB," *IEEE Trans. Geosci. Remote Sens.*, vol. 49, no. 4, pp. 1177–1189, Apr. 2011.
[39] A. Mialon, J.-P. Wigneron, P. De Rosnay, M. J. Escorihuela, and Y. H. Kerr, "Evaluating the L-MEB model from long-term microwave measurements over a rough field, SMOSREX 2006," *IEEE Trans. Geosci. Remote Sens.*, vol. 50, no. 5, pp. 1458–1467, May 2012.
[40] H. Lawrence, J. P. Wigneron, F. Demontoux, A. Mialon, and Y. Kerr, "Evaluating the semi-empirical H-Q model, used to calculate the emissivity of a rough bare soil, with a numerical modeling approach," *IEEE Trans. Geosci. Remote Sens.*, vol. 51, no. 7, pp. 4075–4084, Jul. 2013.
[41] R. Panciera *et al.*, "Evaluation of the SMOS L-MEB passive microwave soil moisture retrieval algorithm," *Remote Sens. Environ.*, vol. 113, no. 2, pp. 435–444, Feb. 2009.
[42] O. Merlin, J. P. Walker, R. Panciera, M. J. Escorihuela, and T. J. Jackson, "Assessing the SMOS soil moisture retrieval parameters with high-resolution NAFE'06 data" *IEEE Geosci. Remote Sens. Lett.*, vol. 6, no. 4, pp. 635–639, Oct. 2009.
[43] H. M. Wainwright, S. Finsterle, Y. Jung, Q. Zhou, and J. T. Birkholzer, "Making sense of global sensitivity analyses," *Comput. Geosci.*, vol. 65, pp. 84–94, Apr. 2014.
[44] J.-C. Calvet *et al.*, "Sensitivity of passive microwave observations to soil moisture and vegetation water content: L-band to W-band," *IEEE Trans. Geosci. Remote Sens.*, vol. 49, no. 4, pp. 1190–1199, Apr. 2011.
[45] K. C. Tien and J. Judge, "Sensitivity of passive microwave observations to soil moisture for growing vegetation," *Appl. Eng. Agric.*, vol. 22, no. 6, pp. 843–850, 2006.
[46] S. Peischl, J. P. Walker, N. Ye, D. Ryu, and Y. Kerr, "Sensitivity of multi-parameter soil moisture retrievals to incidence angle configuration," *Remote Sens. Environ.*, vol. 143, pp. 64–72, Mar. 2014.
[47] C. Ma, X. Li, and S. Wang, "A global sensitivity analysis of soil parameters associated with backscattering using the advanced integral equation model," *IEEE Trans. Geosci. Remote Sens.*, vol. 53, no. 10, pp. 5613–5623, Oct. 2015.
[48] M. Neelam and B. P. Mohanty, "Global sensitivity analysis of the radiative transfer model," *Water Resourc. Res.*, vol. 51, no. 4, pp. 2428–2443, Apr. 2015.
[49] A. Saltelli, S. Tarantola, and K.-S. Chan, "A quantitative model-independent method for global sensitivity analysis of model output," *Technometrics*, vol. 41, no. 1, pp. 39–56, Feb. 1999.
[50] J. R. Wang, P. E. O'Neill, T. J. Jackson, and E. T. Engman, "Multifrequency measurements of the effects of soil moisture, soil texture, and surface roughness," *IEEE Trans. Geosci. Remote Sens.*, vol. GE-21, no. 1, pp. 44–51, Jan. 1983.
[51] M. C. Dobson, F. T. Ulaby, M. T. Hallikainen, and M. A. El-Rayes, "Microwave dielectric behavior of wet soil—Part II: Dielectric mixing models," *IEEE Trans. Geosci. Remote Sens.*, vol. GE-23, no. 1, pp. 35–46, Jan. 1985.
[52] V. L. Mironov, L. G. Kosolapova, and S. V. Fomin, "Physically and mineralogically based spectroscopic dielectric model for moist soils," *IEEE Trans. Geosci. Remote Sens.*, vol. 47, no. 7, pp. 2059–2070, Jul. 2009.
[53] B. Choudhury, T. Schmugge, and T. Mo, "A parameterization of effective soil temperature for microwave emission," *J. Geophys. Res., Oceans*, vol. 87, no. C2, pp. 1301–1304, Feb. 1982.
[54] B. K. Hornbuckle and A. W. England, "Diurnal variation of vertical temperature gradients within a field of maize: Implications for satellite microwave radiometry," *IEEE Geosci. Remote Sens. Lett.*, vol. 2, no. 1, pp. 74–77, Jan. 2005.
[55] A. A. Chukhlantsev, *Microwave Radiometry of Vegetation Canopies*. Dordrecht, The Netherlands: Springer-Verlag, 2006.
[56] T. Jackson and T. Schmugge, "Vegetation effects on the microwave emission of soils," *Remote Sens. Environ.*, vol. 36, no. 3, pp. 203–212, Jun. 1991.
[57] A. A. Van de Griend and J.-P. Wigneron, "The b-factor as a function of frequency and canopy type at H-polarization," *IEEE Trans. Geosci. Remote Sens.*, vol. 42, no. 4, pp. 786–794, Apr. 2004.
[58] A. Saltelli and R. Bolado, "An alternative way to compute Fourier amplitude sensitivity test (FAST)," *Comput. Stat. Data Anal.*, vol. 26, no. 4, pp. 445–460, Feb. 1998.
[59] I. M. Sobol', "On sensitivity estimation for nonlinear mathematical models," *Math. Model. Comput. Exp.*, vol. 2, no. 1, pp. 407–414, 1993.
[60] J. Wang, X. Li, L. Lu, and F. Fang, "Parameter sensitivity analysis of crop growth models based on the extended Fourier amplitude sensitivity test method," *Environ. Model. Softw.*, vol. 48, pp. 171–182, Oct. 2013.
[61] P. Sanadhy, J. Gironás, and M. Arabi, "Global sensitivity analysis of hydrologic processes in major snow-dominated mountainous river basins in Colorado," *Hydrol. Process.*, vol. 28, no. 9, pp. 3404–3418, Apr. 2014.
[62] M. J. Escorihuela, A. Chanzy, J. Wigneron, and Y. Kerr, "Effective soil moisture sampling depth of L-band radiometry: A case study," *Remote Sens. Environ.*, vol. 114, no. 5, pp. 995–1001, May 2010.

Zengyan Wang was born in Jiyuan, Henan, China, in 1987. She received the B.S. degree in cartography and geography information system (GIS) from Henan University, Henan, China, in 2009 and the M.S. degree in cartography and GIS from the Graduate University, Chinese Academy of Sciences (University of Chinese Academy of Sciences), Beijing, China, in 2012, where she is currently working toward the Ph.D. degree in cartography and GIS.

Her research interests include optical and microwave remote sensing, estimation of soil moisture by multisource observations, and related validation issues.

Tao Che received the Ph.D. degree from the Cold and Arid Regions Environmental and Engineering Research Institute (CAREERI), Chinese Academy of Sciences (CAS), Lanzhou, China, in 2006.

Since 2014, he has been a Senior Research Scientist with CAREERI, CAS. His research interests include the remote sensing of land surface parameters in cold and arid regions.

Yuei-An Liou (S'91–M'96–SM'01) received the B.S. degree in electrical engineering from National Sun Yat-Sen University (NSYSU), Kaohsiung, Taiwan, in 1987 and the M.S.E. degree in electrical engineering (EE), the M.S. degree in atmospheric and space sciences, and the Ph.D. degree in EE and atmospheric, oceanic, and space sciences from the University of Michigan, Ann Arbor, MI, USA, in 1992, 1994, and 1996, respectively.

From 1989 to 1990, he was a Research Assistant with the Robotics Laboratory, National Taiwan University, Taipei, Taiwan. From 1991 to 1996, he was a Graduate Student Research Assistant with the Radiation Laboratory, University of Michigan, where he developed land–air interaction and microwave emission models for prairie grassland. He joined the faculty of the Center for Space and Remote Sensing Research (CSRSR) in 1996 and the Institute of Space Sciences in 1997 at the National Central University (NCU), where he is now a Distinguished Professor. He was honored as a Distinguished Professor of NCU in 2010 and 2013. He served as the Division Director of the Science Research Division, National Space Organization (NSPO), Taiwan, in 2005 and continued to serve as an Advisor to NSPO in 2006. From August 2006 to July 2007, he was a Chair Professor and the Dean of the College of Electrical Engineering and Computer Science, Chien Hsin University, Taoyuan, Taiwan. From 2007 to 2010, he served as the Director of CSRSR, NCU. He is currently the President of the Taiwan Group on Earth Observations (2010) and the President of the Taiwan GIS Center (2014). He is a Principal Investigator of many research projects sponsored by the Ministry of Science and Technology (MOST) and Council of Hakka Affairs of Taiwan. He has over 100 referral papers and more than 200 international conference papers. His current research activities include GPS meteorology and ionosphere; remote sensing of the atmosphere, land surface, and polar ice; and land surface process modeling.

Dr. Liou is a member of the American Geophysical Union, the American Meteorological Society, and the International Association of Hydrological Sciences. He was awarded as an Honorary Life Member of The Korean Society of Remote Sensing in 2007. He was elected as a Foreign Member of the Russian Academy of Engineering Sciences in 2008. He was elected as a corresponding member/member of the International Academy of Astronautics in 2009/2014. He is a Referee of the IEEE TRANSACTIONS ON GEOSCIENCE AND REMOTE SENSING (TGRS), *International Journal of Remote Sensing*, *Earth, Planets and Space*, *Remote Sensing of the Environment*, *Journal of Geophysical Research*, *Annales Geophysicae*, etc. He has been a member of the Editorial Advisory Board of *GPS Solutions* since 2001 and *International Journal of Navigation and Observation* since 2011. He has been an Editor of the *Journal of Aeronautics, Astronautics and Aviation* since 2009 and an Associate Editor of *Remote Sensing Technology and Application* since 2011, and he was an Associate Editor of the IEEE JOURNAL OF SELECTED TOPICS IN APPLIED EARTH OBSERVATIONS AND REMOTE SENSING (JSTARS) in 2008–2014. Also, he is a lead guest editor for special issues (*GPS Solutions* in 2005 and 2010, IEEE TRANSACTIONS ON GEOSCIENCE AND REMOTE SENSING in 2008, *Terrestrial, Atmospheric and Oceanic Sciences* in 2014, *Advances in Meteorology* in 2014 and 2015, and *Atmospheric Research, and Remote Sensing* in 2015). He was a recipient of Annual Research Awards from NSC in 1998–2000, a recipient of The First Class Research Awards from NSC in 2004–2006, and a recipient of NCU Outstanding Research Awards in 2004 and 2006–2008. He was awarded the "Contribution Award to FORMOSAT3 National Space Mission" by NSPO in 2006. He was awarded Outstanding Alumni Awards by the University of Michigan Alumni Association in Taiwan and NSYSU in 2008.